Massive multi-missions statistical study and analytical modeling of the Earth magnetopause: 3- An asymmetric non indented magnetopause analytical model

G. Nguyen [1], N.Aunai [1], B.Michotte de Welle [1], A.Jeandet [1], B.Lavraud [2,3] and D.Fontaine [1]

[1]CNRS, Ecole polytechnique, Sorbonne Université, Univ Paris Sud, Observatoire de Paris, Institut Polytechnique de Paris, Université Paris-Saclay, PSL Research Univsersity, Laboratoire de Physique des Plasmas, Palaiseau, France
[2]Laboratoire d'astrophysique de Bordeaux, Univ. Bordeaux, CNRS, B18N, alle Geoffroy Saint-Hilaire, 33615 Pessac, France
[3]Institut de Recherche en Astrophysique et Plantologie, Universit de Toulouse, CNRS, CNES, Toulouse, France

Key Points:

- We use a multi-mission crossings catalog to develop a new asymmetric, non-indented magnetopause surface model.
- The model is parametrized by the upstream solar wind dynamic and magnetic pressures, by the IMF clock angle and by the Earth dipole tilt angle.
- The model provides a more accurate prediction of the magnetopause location than current Magnetopause surface models, especially on the night side of the magnetosphere.

Corresponding author: Gautier Nguyen, gautier-mahe.nguyen@intradef.gouv.fr

Abstract

In a companion statistical study, we showed that the expression of the magnetopause surface as a power law of an elliptic function of the zenith angle θ holds at lunar distances, that the flaring of the magnetopause surface is influenced by the Interplanetary Magnetic Field (IMF) B_y component and that the IMF B_x component had no influence on the stand-off distance.

As a follow-up to these statistical results, this paper presents a new empirical analytical asymmetric and non-indented model of the magnetopause location and shape. This model is obtained from fitting of 15 349 magnetopause crossings using 17 different spacecraft and is parametrized by the upstream solar wind dynamic and magnetic pressures, the IMF clock angle and the Earth dipole tilt angle.

The constructed model provides a more accurate prediction of the magnetopause surface location than current Magnetopause surface models, especially on the night side of the magnetosphere.

1 Introduction

The empirical modeling of the Earth's magnetopause surface as a function of solar wind plasma and magnetic field parameters has been an important topic from the very first discovery of this boundary (Spreiter & Briggs, 1962) until very recently (Nmeek et al. (2020); Hasegawa (2012) and references therein).

Assuming a quadric shape of this boundary, Fairfield (1971) and Formisano (1979) developed the very first magnetopause surface model fitted with in-situ IMP observations.

These early observations also showed that reconnection eroded the magnetosphere in a location that depends on the orientation of the Interplanetary Magnetic Field (IMF) resulting in an earthward motion and in the decrease of the level of flaring for a southward orientation. From then on, numerous analytical empirical models based on a quadric surface, which coefficients depend on both the solar wind dynamic pressure and the IMF B_z component, were fitted using the observations of a single mission at a time (Sibeck et al., 1991; Petrinec et al., 1991; Petrinec & Russell, 1993; Roelof & Sibeck, 1993; Petrinec & Russell, 1996).

Using the observations of several missions simultaneously (IMP and ISEE), Shue et al. (1997) fitted the magnetopause radial distance as the power law of an elliptic function of the zenith angle θ and developed one of the most popular existing model for its simplicity to use and its accuracy.

Despite of this popularity, this model assumes axisymmetry around the Sun-Earth axis, an assumption later questioned by the evidence of seasonal variations of the magnetopause shape by the Hawkeye observations of Boardsen et al. (2000) and Eastman et al. (2000) and by the Interball observations of Šafránková et al. (2002).

This finding, along with the suggestion of a dawn-dusk asymmetry by Kuznetsov and Suvorova (1998), led Lin et al. (2010) to fit their magnetopause surface model using crossings observed from the data of 10 different missions. In addition to considering these two asymmetries, their model also comes with an analytical description of the near-cusp magnetopause in the form of an inward indentation, parametrized by the IMF B_z and the dipole tilt angle. Other parameters such as the full clock angle or the cone angle were not considered yet their effect on the near-cusp magnetopause is unknown. Their expression of the near-cusp indentation furthermore has the drawback of being non-negligible far from the cusp and modifies the interpretation of the terms otherwise controlling the stand-off distance of the level of flaring.

Some years later, Wang et al. (2013) developed a non-analytical model resulting from a support vector regression applied to the combined crossings of 23 different spacecraft. Just assuming the dawn dusk and the seasonal symmetries of the magnetopause, they recovered the dependencies on the dynamic pressure and the IMF B_z. However, neither their data nor their model is shared, the study is consequently hardly reproducible for comparison purposes.

In parallel to these observational studies, Liu et al. (2015) used the magnetopause detected in MagnetoHydroDynamics (MHD) simulations to adapt the model of Shue et al. (1997) to the North-South asymmetry of the magnetopause. Compared to Lin et al. (2010), this model has the advantage of taking into account the influence of the three components of the IMF while predicting the magnetopause with a slightly increased accuracy (Liu et al., 2015). Nevertheless, their model indicates that an increasing IMF B_x induces a North-South asymmetry, which is in opposition with the observational findings of Dušík et al. (2010) or Grygorov et al. (2017) who rather suggested a sunward motion of the magnetopause. Furthermore, the crossings used for the observational comparison with Lin et al. (2010) were by far mostly located in the dayside northern hemisphere region which thus gives poor evidence on how the model performs in the southern hemisphere or at lunar distances.

Using automatically detected events along with observations manually selected by various experts, Nguyen et al. (2020b) performed a statistical analysis of the position of 15 349 magnetopause crossings that came from 10 different missions. This study confirmed well-known properties of the magnetopause such as the influence of the solar wind dynamic pressure, the seasonal variation or the influence of the IMF B_z component. They also showed that the expression of the magnetopause surface as a power law of an elliptic function of the zenith angle θ was still holding at lunar distances and evidenced the influence of the IMF GSM clock angle on the flaring level. Their investigations also suggested the absence of a sunward motion of the magnetopause with an increasing IMF B_x component.

In this third paper of a series of papers dedicated to the magnetopause, we develop a new asymmetric, non-indented analytical magnetopause model that takes into consideration these latest findings.

The outline of this paper is as follows: Section 2 presents the magnetopause crossings dataset we use and the associated upstream solar wind and IMF conditions, Section 3 focuses on the development of the magnetopause model, Section 4 compares it with other existing magnetopause models and Section 5 presents its differents characteristics.

2 Dataset

We use the same magnetopause crossings dataset as that presented in Nguyen et al. (2020b). This dataset consists in the combination of 13 181 magnetopause crossings detected in the data of the most recent near-Earth missions (THEMIS, Cluster, Double Star, ARTEMIS and MMS) with a gradient boosting classifier (see Nguyen et al. (2020a) for more details) [1] together with the 2168 events manually identified by various experts in the data of older missions (OGO, Geotail, Hawkeye, AMPTE and IMP). [2]

The solar wind upstream conditions associated to each crossings were obtained from OMNI data by applying the two-step propagation algorithm exposed in Šafránková et al. (2002).

[1] Such crossings can be found online at : `https://github.com/gautiernguyen/in-situ_Events_lists`

[2] Such crossings can be found online at : `ftp://nssdcftp.gsfc.nasa.gov/spacecraftdata/magnetopausecrossings)`

In order to remove the aberration caused by the Earth's revolution, we correct the GSM position of each crossing by using a similar approach than Lin et al. (2010) and Boardsen et al. (2000), assuming a revolution velocity of 30 km/s.

In addition to the non-aberrated GSM (X, Y, Z) cartesian coordinates, we use the spherical counterpart (R, θ, ϕ) as in Nguyen et al. (2020b):

$$\begin{cases} X = R\cos(\theta) \\ Y = R\sin(\theta)\sin(\phi) \\ Z = R\sin(\theta)\cos(\phi) \end{cases} \tag{1}$$

Similarly to Wang et al. (2013) and Nguyen et al. (2020b), we balance the hemispheric distribution of the dataset by assuming a symmetry between the summer northern hemisphere and the winter southern hemisphere and thus by reverting the GSM Z coordinate and the Earth dipole tilt angle γ: : $r(X, Y, Z, \gamma) = r(X, Y, -Z, -\gamma)$.

Following the suggestions of Nguyen et al. (2020b) we also assume a dawn-dusk symmetry of the magnetopause and thus revert the Y component of each event.

Different observations of the polar cusps crossings led to different conclusions regarding the shape of the boundary in the near-cusp region. Boardsen et al. (2000); Šafránková et al. (2002); afrnkov et al. (2005) suggested the magnetopause is indented while Zhou and Russell (1997); Lavraud et al. (2004) suggested a non-indented boundary. This question is investigated in the fourth paper of our study (Nguyen et al., 2020c). For now, we restrict the dataset to the 58154 so-called "out of cusp" events. Those events are defined as those falling outside of the cusp indentation as defined by Lin et al. (2010), for which θ satisfies:

$$\begin{cases} (\theta - \theta_n)^2 + \phi^2 \geq \left(-\frac{1}{d_n}\right)^{\frac{2}{a_{21}}} \text{ if } Z \geq 0 \\ (\theta - \theta_s)^2 + \phi^2 \geq \left(-\frac{1}{d_s}\right)^{\frac{2}{a_{21}}} \text{ if } Z \leq 0 \end{cases} \tag{2}$$

Where $d_{n,s} = a_{16} \pm a_{17}\gamma + a_{18}\gamma^2$, $\theta_{n,s} = a_{19} \pm a_{20}\gamma$, and a_{21} represent the scope, the zenithal position and the shape of the polar cusps, γ is the Earth dipole tilt angle and $a_{16}, a_{17}, a_{18}, a_{19}, a_{20}$ and a_{21} are the corresponding coefficients fitted by Lin et al. (2010). The crossings that are found inside of this so-defined cusp-indentation will constitute the core of the dataset used in Nguyen et al. (2020c).

The obtained symmetrized dataset is randomly split into a training set 43 664 events that will serve for the fit performed in section 4 and into a test set of 14 490 events used to evaluate the accuracy of the resulting model in section 5.

The distribution of the cartesian position and the associated solar wind physical parameters of the events that constitute the different sets is shown in Figure 1.

In each panel, we notice similar distributions of both the train and the test sets. This indicates that there is no particular bias between the two sets.

3 Construction of the magnetopause model

Previous statistical studies of the magnetopause location and shape (Shue et al., 1997; Liu et al., 2015; Nguyen et al., 2020b) confirmed the relevance of the analytical definition of the magnetopause surface as the power law of an elliptic function. Thus, we keep this basis for the construction of our model:

$$r = r_0 \left(\frac{2}{1 + \cos(\theta)}\right)^{\alpha} \tag{3}$$

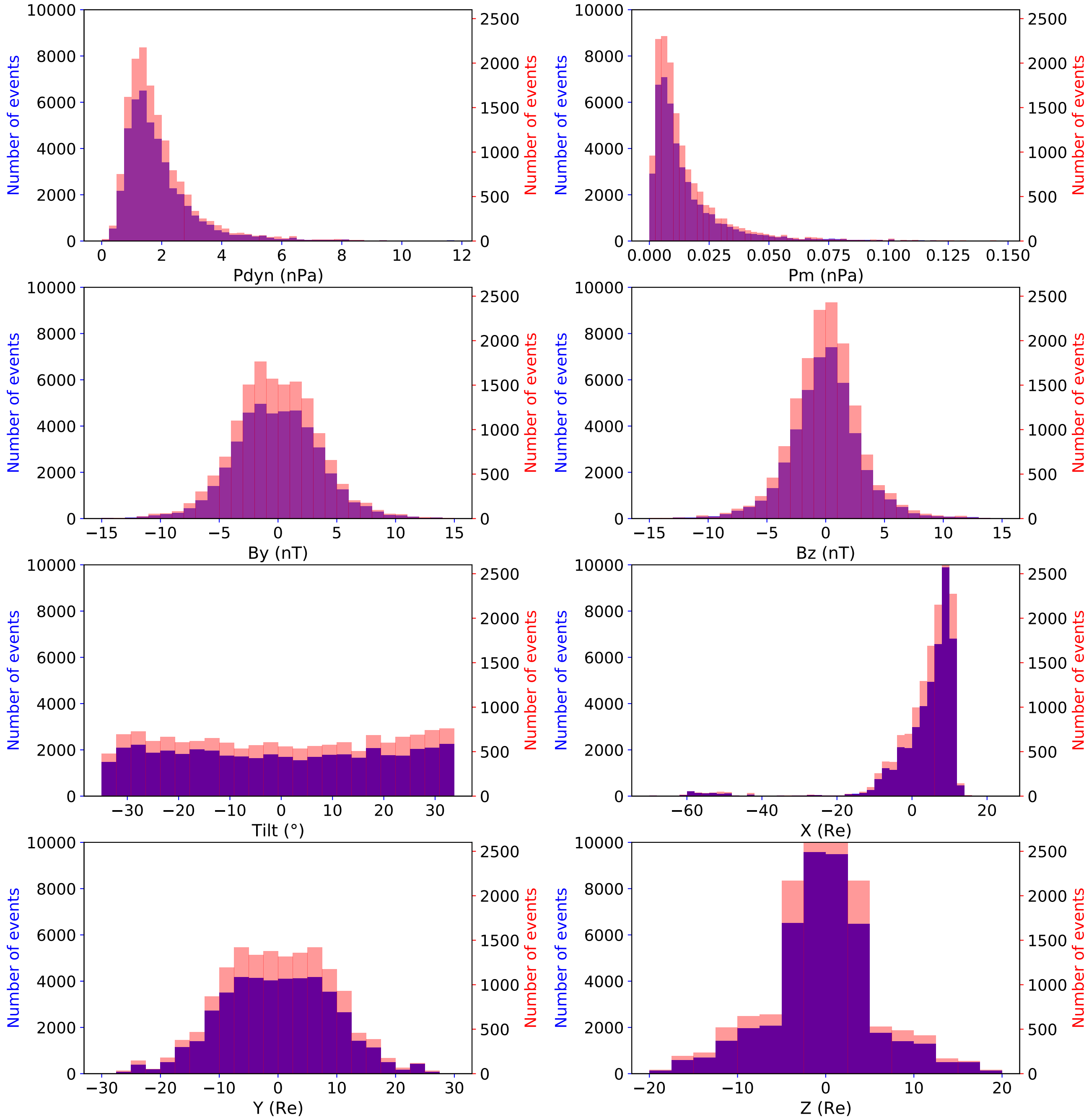

Figure 1. Histogram of the solar wind parameters and the cartesian position of the 43 664 events of the train set (blue) and of the 14 490 events of the test set (*blue red*): the dynamic pressure P_{dyn} (*top left*), the magnetic pressure P_m (*top, right*), the IMF B_y and B_z components (*second row, left and right*), the Earth dipole tilt angle γ (*third row, left*) and the GSM cartesian position, X (*third row, right*), Y and Z (*last row, left and right*).

Where r_0 describes the position of the magnetopause nose and α controls the level of tail flaring.

Following the results of Nguyen et al. (2020b), we define r_0 as:

$$r_0 = a_0(P_{dyn} + P_m)^{a_1}(1 + a_2 \tanh(a_3 B_z) + a_4) \tag{4}$$

In the case of an axisymmetric magnetopause, α is independant from the zenith and the azimuth angles, θ and ϕ. The assumption, espacially made by Shue et al. (1997), is however not true as the most recent statistical studies (Nguyen et al. (2020b) and references therein) evidenced an azimuthal and a north-south asymmetry of the magnetopause induced by the IMF B_y and B_z components and by the Earth dipole tilt angle, respectively.

Consequently, we define the flaring level as:

$$\begin{cases} \alpha = \alpha_0 + \alpha_1 \cos(\phi) + \alpha_2 \cos(\phi)^2 + \alpha_3 \sin(\phi)^2 \\ \alpha_0 = a_5 \\ \alpha_1 = a_6 \gamma \\ \alpha_2 = a_7 \cos(\Omega) \\ \alpha_3 = a_8 \cos(\Omega) \end{cases} \tag{5}$$

Where α_0 is the average level of flaring expected in the case of an axisymmetric magnetopause. α_1 describes the north-south asymmetry induced by seasonal variations through the variation of the dipole tilt angle γ . α_2 (resp. α_3) describes the variations of the magnetopause in the $(X - Z)$ (resp. $(X - Y)$) plane induced by the variations of the IMF clock angle Ω.

The values of the 9 a_i coefficients are initially set with the fitting values found in Nguyen et al. (2020b). a_0, a_1, a_2, a_3 and a_4 are predetermined by fitting (4) to the 275 events for which $\theta < 7.750°$ and $Z > 0$. The initial values of a_5 and a_7 are determined by fitting 3, 4, 5, to the 5170 out of cusps crossings for which $|Z| < 1$ *Re* and assuming all of these events belong to the $(X - Y)$ plane. The initial values of a_5, a_6 and a_8 are determined by fitting 3, 4, 5 to the 2154 out of cusps crossings for which $|Y| < 2$ *Re* assuming all of these events belong to the $(X - Z)$ plane. The initial fitting values are shown in Table 1.

a_0	a_1	a_2	a_3	a_4	a_5	a_6	a_7	a_8
10.75	-0.161	0.050	0.35	1.60	0.55 , 0.51	0.026	0.015	-0.050

Table 1. Initial values of the coefficients of the equations 3 to 5 obtained from the initial fits around the subsolar point of a_0, a_1, a_2, a_3 and a_4, in the $(X - Y)$ plane for a_5 (*first value*) and a_7 and in the $(X - Z)$ plane for a_5 (*second value*), a_6 and a_8

The final values of the 9 a_i coefficients are then obtained by applying the Levenberg-Marquardt fitting method (Newville et al., 2014) on the 43 664 events of the training set and are presented in the Table 2.

This fitting phase then results in an analytical empirical model of the non-indented magnetopause shape and location that depends on the solar wind total pressure $P_{dyn} + P_m$, the IMF B_z and clock angle Ω and the dipole tilt angle γ. A numerical implementation of this model can be found at: `https://github.com/gautiernguyen/magnetopause_models` and will be the one used in the following paragraphs.

a_0	a_1	a_2	a_3	a_4	a_5	a_6	a_7	a_8
10.73	-0.150	0.0208	0.38	2.09	0.55	0.088	0.015	-0.087

Table 2. Final values of the coefficients a_i of the equations 3 to 5 obtained after a total fit on the training set.

	Our model	Liu et al. (2015)	Lin et al. (2010)	Shue et al. (1997)
$X < -30$ (361)	6.06 ± 0.32	15.01 ± 0.53	14.06 ± 0.34	9.19 ± 0.34
$X > -30$ and $X < 0$ (2525)	1.67 ± 0.033	2.39 ± 0.040	2.48 ± 0.047	2.26 ± 0.034
$X > 0$ and $\|Z\| > 7.5$ (1188)	1.84 ± 0.042	1.78 ± 0.042	1.72 ± 0.044	2.24 ± 0.043
$X > 0$ and $\|Z\| < 7.5$ and $\|Y\| > 7.5$ (3992)	1.02 ± 0.016	0.99 ± 0.017	1.22 ± 0.016	1.19 ± 0.016
$X > 0$ and $\|Z\| < 7.5$ and $\|Y\| > 7.5$ (6424)	0.93 ± 0.011	0.86 ± 0.010	0.96 ± 0.010	1.00 ± 0.012
All regions (14490)	1.53 ± 0.013	2.73 ± 0.021	2.65 ± 0.023	2.06 ± 0.015

Table 3. RMSE of the different models in different region for he 14490 crossings of the test set, the uncertainty represents the standard error of mean of the error of each model. The number between brackets in the first column indicate the number of events per region.

4 Comparison with other models

We evaluate the accuracy of the fitted model by computing its Root Mean Square Error (RMSE) on the 14490 events of the test set and compare it to the RMSE of the models of Shue et al. (1997), Lin et al. (2010) and Liu et al. (2015) computed on the same test set. To keep a consistent comparison, we removed the indentation part of the models of Lin et al. (2010) and Liu et al. (2015) during the computation of the RMSE. The score we obtain for the different models for different spatial regions are shown in the Table 3 and visually represented in the Figure 2.

The obtained RMSE in the low-latitude, dayside, subsolar and flank regions, is almost similar for the four models, this indicates that our model provides an accurate description of the magnetopause shape and location in those regions and this is not surprising given the proximity of the expression and coefficients of the stand-off distance of the 4 models. At high latitudes, we notice a more important error for the model of Shue et al. (1997) that is not surprising as no high latitude data was considered during the development of this model and this is particularly reflected by the similarity we find between our RMSE and the RMSE of Lin et al. (2010) and Liu et al. (2015).

Looking at the "close" nightside region, we notice this time a reduced error of our model in comparison to the three others, than can be explained by our consideration of the IMF clock angle in the expression of the flaring coefficient α rather than the lone B_z.

Finally, the previous models were established without consideration of magnetopause crossings further than -30 Re, especially the one detected by ARTEMIS and it is thus not surprising to notice a lower RMSE for our model in the "far" nightside. Naturally, the error here is possibly substantially higher than in any other region we considered. This could be explained by the flapping of the magnetotail in the far nightside that could result in a much more variable boundary(Sergeev et al., 1998). As the position of the magnetopause does not rely on the solar wind physical parameters alone but also on the magnetotail dynamics, this necessarily constitute a non negligible source of errors.

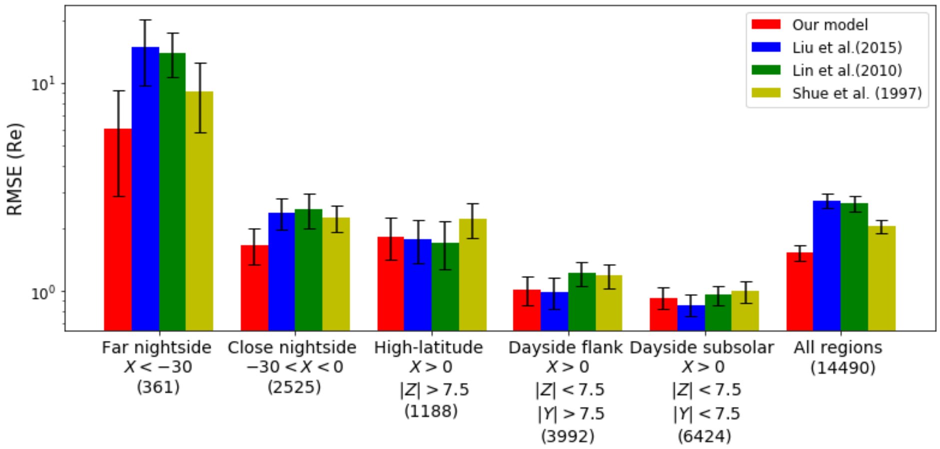

Figure 2. Visual representation of the RMSE of the different models exposed in the Table 3. The error bar represent 10 times the Standard Error of the Mean of the error made by the models on the test set.

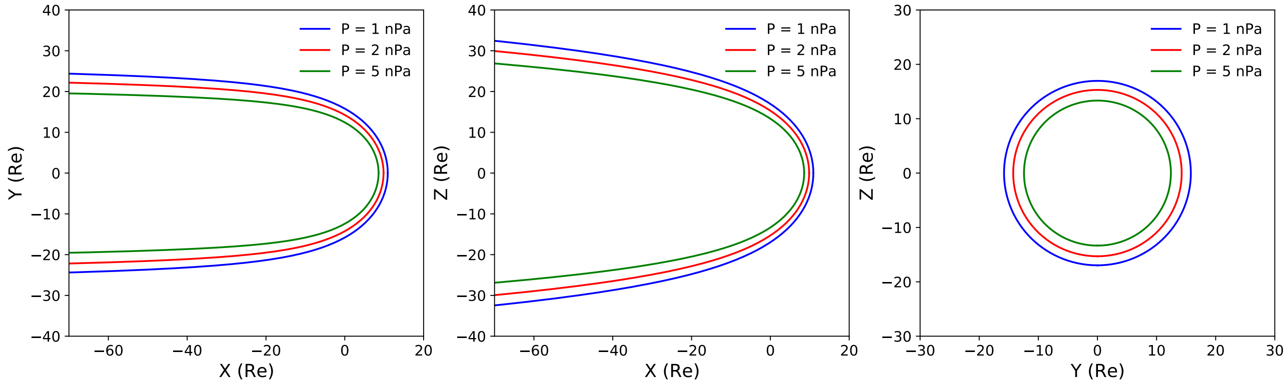

Figure 3. Projection in the $(X-Y)$ (*left*), $(X-Z)$ (*middle*), and $(Y-Z)$ (*right*) planes of our model for varying total pressure $P = P_{dyn} + P_m$. The IMF is purely southward and B_z = -2 nT.

Combining the regions altogether (last group of bars of Figure 2), we obtain a global RMSE that is lower for our model in comparison to the others and thus ensures the reliability of our model and its legitimacy to be exploited in further magnetopause studies.

5 Characteristics of the model

We show the influence of the total pressure, $P = P_{dyn} + P_m$ on our magnetopause model with the three panels of Figure 3. Following what we evidenced in Nguyen et al. (2020b), the total pressure pushes the magnetopause earthward along the X axis without influencing the flaring. This behavior confirms the findings of the previous models that showed very little pressure dependency of the flaring. Additionally, we find a power law index a_1 equal to -0.15 that is very close to the theoretical $-1/6$ for a dipole in vacuum and in the same orders of magnitude than the values found by Shue et al. (1997), Lin et al. (2010) and Liu et al. (2015).

The three panels of Figure 4 that represent the influence of the IMF clock angle. Following the suggestions of Nguyen et al. (2020b), the model results in an elliptic magnetopause YZ cross section on the Z axis for negative B_z. This direction change is consistent

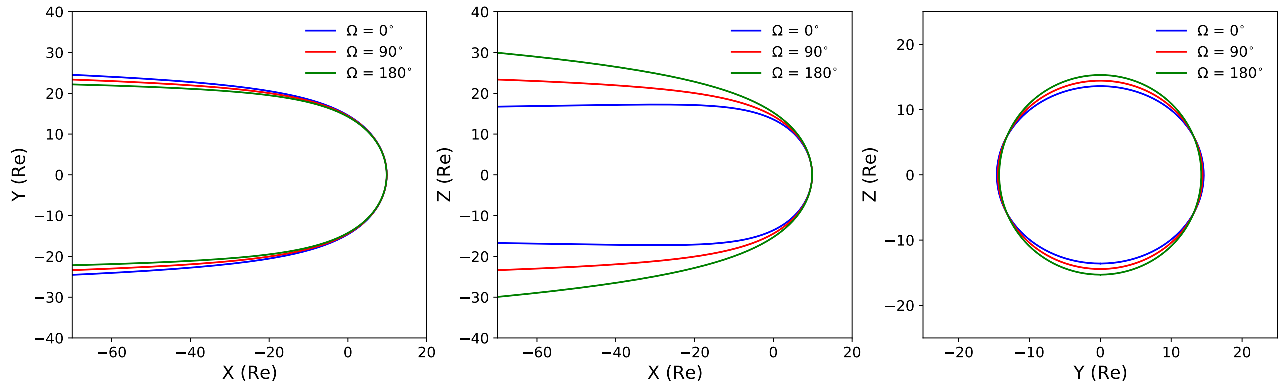

Figure 4. Projection in the $(X-Y)$ (*left*), $(X-Z)$ (*middle*), and $(Y-Z)$ (*right*) planes of our model for varying clock angle Ω. The total pressure is equal to 2 nPa and $|B| = 2$nT.

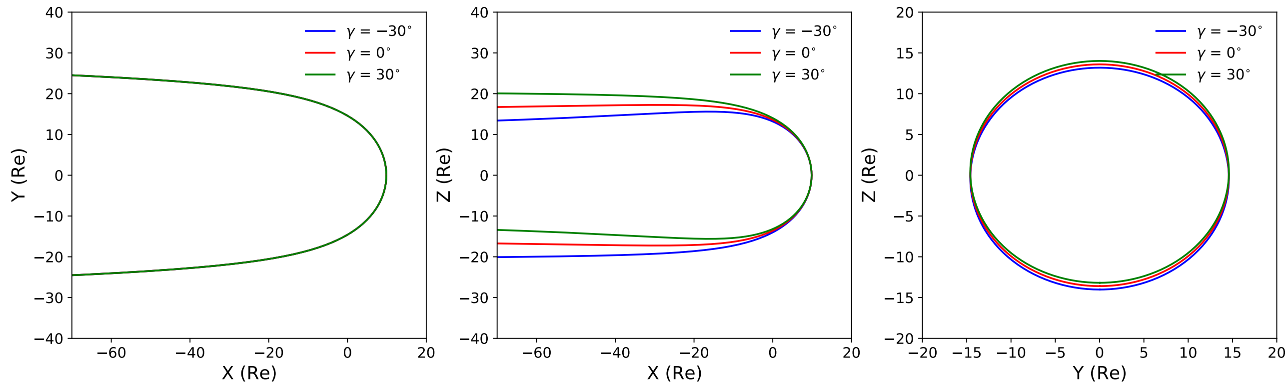

Figure 5. Projection in the $(X-Y)$ (*left*), $(X-Z)$ (*middle*), and $(Y-Z)$ (*right*) planes of our model for varying dipole tilt angle γ. The total pressure is equal to 2 nPa, the IMF is purely northward and and $B_z = 2$nT .

with the one obtained by (Wang et al., 2013) and could be explained by the tail accumulation of newly reconnected field line that appears in the case of a southward IMF, resulting in an enhanced level of flaring.

We show the influence of the dipole tilt angle γ with the three panels of Figure 5 that clearly indicates a magnetopause that rotates around the Y axis with a rotating dipole tilt angle resulting in a north hemisphere summer (respectively south hemisphere winter) shift of the magnetopause cross section.

Finally, computing the magnetopause location at all angles for the same solar wind conditions results in a misleading picture. The different existing magnetopause surface models return a static representation of the magnetopause for a permanent upstream solar wind regime. Actually, the magnetopause has a dynamic motion that follows the variations of the upstream solar wind. For this reason, it would be interesting to adapt the existing static model into a dynamic expression of the magnetopause surface able to give an estimation of the magnetopause shape and location at any time. A simple description of such adaptation to our model that only consider different upstream solar wind conditions for the different points of the surface can especially be found in the appendix A.

6 Conclusion

In this paper, we exploit the statistical findings of Nguyen et al. (2020b), a companion study, to develop a new asymmetric non indented magnetopause surface model. Just like the past existing studies (Shue et al., 1997; Lin et al., 2010; Liu et al., 2015), our model is expressed as the power law of an elliptic function of the GSM zenith angle θ and is here parameterized by the upstream solar wind dynamic and magnetic pressure, by the IMF clock angle and by the Earth dipole tilt angle.

Comparing our model with the models of Shue et al. (1997), Lin et al. (2010) and Liu et al. (2015), we found the 4 models to predict the magnetopause location with similar accuracy on the dayside equatorial part of the magnetopause and the error made by our model is similar to the one made by Lin et al. (2010) and Liu et al. (2015) on the high-latitude dayside part of the magnetopause. On the nightside, the consideration of crossings farther downtail than -30 Re resulted in a reduced error in comparison to the other existing models. Nevertheless, the lack of data in this region combined to the much more variable nature of the magnetopause at such distances (Sergeev et al., 1998) indicate further studies are needed in this specific region of the near-Earth environment.

Assuming a dawn-dusk symmetry of the magnetopause, our model predicts a magnetopause squeezed or stretched in the Y or Z direction, respectively, when the IMF turns from a northward to a southward orientation. This finding gives clues on the influence of the Y component of the IMF on the magnetopause and is in agreement with Liu et al. (2015). However, for statistical reasons, we limited our study to the $(X - Y)$ and the $(X - Z)$ and symmetrized our dataset. As a consequence, neither the statistical investigations we performed in Nguyen et al. (2020b) nor the model we developed in this paper considered a continuous twist of the magnetopause with the IMF clock angle as suggested by Liu et al. (2015) and Lavraud and Borovsky (2008). Future investigations, using more data, should address this delicate point.

Finally, all of the crossings we used in this paper were located outside of the near-cusp regions and there is thus no clue on how well our non-indented model performs and the extent to which it has to be adapted in order to provide a precise description of the magnetopause in this specific region of the near-Earth environment. This issue is addressed in Nguyen et al. (2020c), the last companion paper of our study.

Appendix A From a static to a dynamic model

All of the existing analytical magnetopause surface model provide a static view of the magnetopause for a given upstream solar wind regime, which is far from being the actual ground truth. This shows the interest we have in adapting the existing static models into their dynamic counterpart.

To do so, we adapt the two-step propagation algorithm of Šafránková et al. (2002) in order to estimate the temporal shift to OMNI data needed for each zenith angle θ along the GSM X axis :

1. At a given time t and a given zenith angle θ, we estimate a first position of the magnetopause by computing our model for the averaged solar wind conditions in the interval between t and $t - 30$ min. We chose 30 minutes as this is the typical shifting time we obtain for $X \sim -70$ Re.
2. This first position serves to estimate a first value of the X coordinate of the magnetopause at this value of θ.
3. We apply the two step propagation algorithm to estimate a first shifting time from this first X position and compute the associated radial position of the magnetopause.

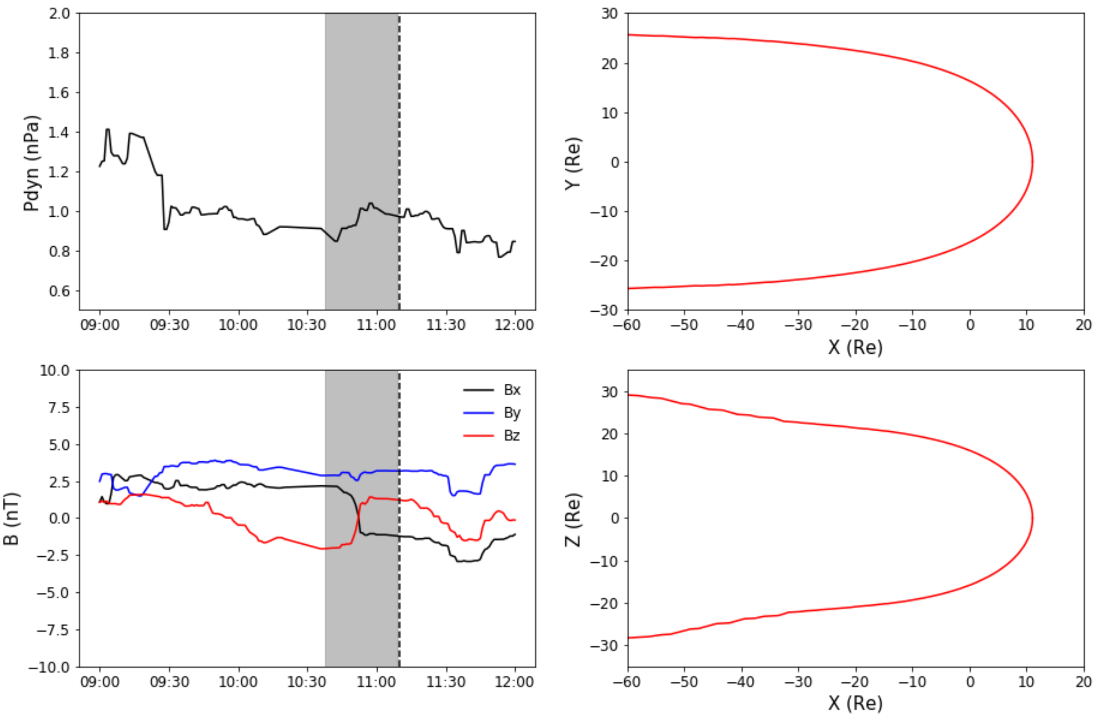

Figure A1. OMNI solar wind dynamic pressure (*top*) and magnetic field (*bottom*) measurement (*left column*) on the 3^{rd} of March 2011 and projection of our dynamical magnetopause model (*right column*) in the $(X-Y)$ (*top*) and in the $(X-Z)$ (*bottom*) planes at the time corresponding to the black dashed line on the left column. The grey interval in the left panels represent the data interval propagated throughout the whole magnetopause.

4. We use this second radial position to re-estimate the X coordinate of the magnetopause at this value of θ.
5. We apply the two-step propagation algorithm a second time to determine the final shifting time that will be used for this value θ and we compute the associated final radial position of the magnetopause.

At a given time t, we apply this process for every zenithal position θ and end up with a dynamical magnetopause model similar to the one shown in the two right panels of Figure A1 where we represented the projection of the magnetopause in the $(X-Y)$ and in the $(X-Z)$ planes at the time indicated by the black dashed line on the two left panels. Naturally, the shifting time increases with the zenith angle and the left boundary of the grey interval represented in the two left panels then corresponds to the magnetopause computed at the left border of the two right panels. The obtained magnetopause then considers an IMF shift from a negative to a positive B_z and the propagation of this transition is reproduced through the propagation of the erosion we notice in the $(X-Z)$ plane.

Adapting the two step propagation algorithm, we then elaborated a process useful for providing a dynamical view of the magnetopause at any time. Additionally, this process is independent from the used static magnetopause model and thus easily adaptable to the models of Shue et al. (1997), Lin et al. (2010) and Liu et al. (2015).

The numerical implementation of this models can be found at: `https://github.com/gautierngyuen/magnetopause_models`

Acknowledgments

Enter acknowledgments, including your data availability statement, here.

References

Boardsen, S. A., Eastman, T. E., Sotirelis, T., & Green, J. L. (2000). An empirical model of the high-latitude magnetopause. *Journal of Geophysical Research: Space Physics*, *105*(A10), 23193-23219. Retrieved from `https://agupubs.onlinelibrary.wiley.com/doi/abs/10.1029/1998JA000143` doi: 10.1029/1998JA000143

Dušík, Š., Granko, G., Šafránková, J., Němeček, Z., & Jelínek, K. (2010, October). IMF cone angle control of the magnetopause location: Statistical study. *Geophysical Research Letters*, *37*(19), L19103. doi: 10.1029/2010GL044965

Eastman, T. E., Sotirelis, T., & Green, J. L. (2000). An Empirical Model of the High-latitude Magnetopause. *Journal of Geophysical Research*, *105*(1998). doi: doi:10.1029/1998JA000143

Fairfield, D. H. (1971, Jan). Average and unusual locations of the Earth's magnetopause and bow shock. *Journal of Geophysical Research*, *76*(28), 6700. doi: 10.1029/JA076i028p06700

Formisano, V. (1979, Dec). The three-dimensional shape of the bow shock. *Planetary and Space Science*, *2C*, 681-692. doi: 10.1007/BF02558125

Grygorov, K., afrnkov, J., Nmeek, Z., Pi, G., Pech, L., & Urb, J. (2017). Shape of the equatorial magnetopause affected by the radial interplanetary magnetic field. *Planetary and Space Science*, *148*, 28 - 34. Retrieved from `http://www.sciencedirect.com/science/article/pii/S0032063317302131` doi: https://doi.org/10.1016/j.pss.2017.09.011

Hasegawa, H. (2012, August). Structure and Dynamics of the Magnetopause and Its Boundary Layers. *Monographs on Environment, Earth and Planets*, *1*(2), 71-119. doi: 10.5047/meep.2012.00102.0071

Kuznetsov, S. N., & Suvorova, A. V. (1998, January). Solar wind magnetic field and pressure during magnetopause crossings at geosynchronous orbit. *Advances in Space Research*, *22*(1), 63-66. doi: 10.1016/S0273-1177(97)01101-0

Lavraud, B., & Borovsky, J. E. (2008). Altered solar wind-magnetosphere interaction at low mach numbers: Coronal mass ejections. *Journal of Geophysical Research: Space Physics*, *113*(A9). Retrieved from `https://agupubs.onlinelibrary.wiley.com/doi/abs/10.1029/2008JA013192` doi: https://doi.org/10.1029/2008JA013192

Lavraud, B., Fedorov, A., Budnik, E., Grigoriev, A., Cargill, P., Dunlop, M., ... Balogh, A. (2004, August). Cluster survey of the high-altitude cusp properties: a three-year statistical study. *Annales Geophysicae*, *22*(8), 3009-3019. doi: 10.5194/angeo-22-3009-2004

Lin, R. L., Zhang, X. X., Liu, S. Q., Wang, Y. L., & Gong, J. C. (2010, Apr). A three-dimensional asymmetric magnetopause model. *Journal of Geophysical Research (Space Physics)*, *115*(A4), A04207. doi: 10.1029/2009JA014235

Liu, Z., Lu, J. Y., Wang, C., Kabin, K., Zhao, J. S., Wang, M., ... Zhao, M. X. (2015). Journal of Geophysical Research : Space Physics A three-dimensional high Mach number asymmetric magnetopause model from global MHD simulation. *Journal of Geophysical Research*, 5645–5666. doi: 10.1002/2014JA020961.Received

Newville, M., Stensitzki, T., Allen, D. B., & Ingargiola, A. (2014, September). *LMFIT: Non-Linear Least-Square Minimization and Curve-Fitting for Python.* Zenodo. Retrieved from `https://doi.org/10.5281/zenodo.11813` doi: 10.5281/zenodo.11813

Nguyen, G., Aunai, N., Michotte de Welle, B., Jeandet, A., Lavraud, B., & Fontaine, D. (2020a). *Massive multi-missions statistical study and analytical modeling of the Earth magnetopause: 1 - A gradient boosting based automatic detection of near-Earth regions.* (Submitted)

Nguyen, G., Aunai, N., Michotte de Welle, B., Jeandet, A., Lavraud, B., & Fontaine, D. (2020b). *Massive multi-missions statistical study and analytical modeling of the Earth* *magnetopause: 2 - Shape and location.* (Submitted)

Nguyen, G., Aunai, N., Michotte de Welle, B., Jeandet, A., Lavraud, B., & Fontaine, D. (2020c). *Massive multi-missions statistical study and analytical modeling of the Earth magnetopause: 4- On the near-cusp magnetopause indentation.* (Submitted)

Nmeek, Z., afrnkov, J., & imnek, J. (2020). An examination of the magnetopause position and shape based upon new observations. In *Dayside magnetosphere interactions* (p. 135-151). American Geophysical Union (AGU). Retrieved from `https://agupubs.onlinelibrary.wiley.com/doi/abs/10.1002/9781119509592.ch8` doi: 10.1002/9781119509592.ch8

Petrinec, S. M., & Russell, C. T. (1993, December). An empirical model of the size and shape of the near-Earth magnetotail. *Geophysical Research Letters*, *20*(23), 2695-2698. doi: 10.1029/93GL02847

Petrinec, S. M., & Russell, C. T. (1996). Near-earth magnetotail shape and size as determined from the magnetopause flaring angle. *Journal of Geophysical Research: Space Physics*, *101*(A1), 137-152. Retrieved from `https://agupubs.onlinelibrary.wiley.com/doi/abs/10.1029/95JA02834` doi: 10.1029/95JA02834

Petrinec, S. P., Song, P., & Russell, C. T. (1991, May). Solar cycle variations in the size and shape of the magnetopause. *Journal of Geophysical Research*, *96*(A5), 7893-7896. doi: 10.1029/90JA02566

Roelof, E. C., & Sibeck, D. G. (1993, December). Magnetopause shape as a bivariate function of interplanetary magnetic field B_z and solar wind dynamic pressure. *Journal of Geophysical Research*, *98*(A12), 21421-21450. doi: 10.1029/93JA02362

Sergeev, V., Angelopoulos, V., Carlson, C., & Sutcliffe, P. (1998). Current sheet measurements within a flapping plasma sheet. *Journal of Geophysical Research: Space Physics*, *103*(A5), 9177-9187. Retrieved from `https://agupubs.onlinelibrary.wiley.com/doi/abs/10.1029/97JA02093` doi: 10.1029/97JA02093

Shue, J. H., Chao, J. K., Fu, H. C., Russell, C. T., Song, P., Khurana, K. K., & Singer, H. J. (1997, May). A new functional form to study the solar wind control of the magnetopause size and shape. *Journal of Geophysical Research*, *102*(A5), 9497-9512. doi: 10.1029/97JA00196

Sibeck, D. G., Lopez, R. E., & Roelof, E. C. (1991, Apr). Solar wind control of the magnetopause shape, location, and motion. *Journal of Geophysical Research*, *96*(A4), 5489-5495. doi: 10.1029/90JA02464

Spreiter, J. R., & Briggs, B. R. (1962). Theoretical determination of the form of the boundary of the solar corpuscular stream produced by interaction with the magnetic dipole field of the earth. *Journal of Geophysical Research (1896-1977)*, *67*(1), 37-51. Retrieved from `https://agupubs.onlinelibrary.wiley.com/doi/abs/10.1029/JZ067i001p00037` doi: 10.1029/JZ067i001p00037

Šafránková, J., Němeček, Z., Dušík, v., Přech, L., Sibeck, D. G., & Borodkova, N. N. (2002). The magnetopause shape and location: a comparison of the interball and geotail observations with models. *Annales Geophysicae*, *20*(3), 301–309. Retrieved from `https://www.ann-geophys.net/20/301/2002/` doi: 10.5194/angeo-20-301-2002

Wang, Y., Sibeck, D. G., Merka, J., Boardsen, S. A., Karimabadi, H., Sipes, T. B., . . . Lin, R. (2013, May). A new three-dimensional magnetopause model with a support vector regression machine and a large database of multiple spacecraft observations. *Journal of Geophysical Research (Space Physics)*, *118*, 2173-2184. doi: 10.1002/jgra.50226

Zhou, X.-W., & Russell, C. T. (1997). The location of the high-latitude polar cusp and the shape of the surrounding magnetopause. *Journal of Geophysical Research: Space Physics*, *102*(A1), 105-110. Retrieved from `https://agupubs.onlinelibrary.wiley.com/doi/abs/10.1029/96JA02702` doi: 10.1029/96JA02702

afrnkov, J., Dusk, ., & Nmeek, Z. (2005). The shape and location of the high-latitude magnetopause. *Advances in Space Research*, *36*(10), 1934 - 1939. Retrieved from `http://www.sciencedirect.com/science/article/pii/S0273117705004795` (Solar Wind-Magnetosphere-Ionosphere Dynamics and Radiation Models) doi: https://doi.org/10.1016/j.asr.2004.05.009